

# Scaling properties of the mean multiplicity and pseudorapidity density in $e^- + e^+$ , $e^\pm + p$ , $p(\bar{p})+p$ , $p+A$ and $A+A(B)$ collisions

Roy A. Lacey,<sup>1,2,\*</sup> Peifeng Liu,<sup>1,2</sup> Niseem Magdy,<sup>1</sup> M.Csanád,<sup>1,3</sup>  
B. Schweid,<sup>1,2</sup> N. N. Ajitanand,<sup>1</sup> J. Alexander,<sup>1</sup> and R. Pak<sup>4</sup>

<sup>1</sup>*Department of Chemistry, Stony Brook University, Stony Brook, NY, 11794-3400, USA*

<sup>2</sup>*Dept. of Physics, Stony Brook University, Stony Brook, NY, 11794, USA*

<sup>3</sup>*Eotvos University, Department of Atomic Physics, H-1117 Budapest, Hungary*

<sup>4</sup>*Brookhaven National Laboratory, Upton, New York 11973, USA*

(Dated: June 9, 2021)

The pseudorapidity density ( $dN_{\text{ch}}/d\eta$ ) for  $p(\bar{p})+p$ ,  $p+A$  and  $A+A(B)$  collisions, and the mean multiplicity  $\langle N_{\text{ch}} \rangle$  for  $e^- + e^+$ ,  $e^\pm + p$ , and  $p(\bar{p})+p$  collisions, are studied for an inclusive range of beam energies ( $\sqrt{s}$ ). Characteristic scaling patterns are observed for both  $dN_{\text{ch}}/d\eta$  and  $\langle N_{\text{ch}} \rangle$ , consistent with a thermal particle production mechanism for the bulk of the soft particles produced in all of these systems. They also validate an essential role for quark participants in these collisions. The scaled values for  $dN_{\text{ch}}/d\eta$  and  $\langle N_{\text{ch}} \rangle$  are observed to factorize into contributions which depend on  $\log(\sqrt{s})$  and the number of nucleon or quark participant pairs  $N_{\text{pp}}$ . Quantification of these contributions give expressions which serve to systematize  $dN_{\text{ch}}/d\eta$  and  $\langle N_{\text{ch}} \rangle$  measurements spanning nearly four orders of magnitude in  $\sqrt{s}$ , and to predict their values as a function of  $\sqrt{s}$  and  $N_{\text{pp}}$ .

PACS numbers: 25.75.Dw

Measurements of particle yields and kinematic distributions in electron-positron ( $e^- + e^+$ ), electron-proton ( $e^\pm + p$ ), proton-proton ( $p(\bar{p})+p$ ), proton-nucleus ( $p+A$ ) and nucleus-nucleus ( $A+A(B)$ ) collisions, are essential for characterizing the global properties of these collisions, and to develop a good understanding of the mechanism/s for particle production [1–9]. The  $p+p$  measurements also provide crucial reference data for studies of nuclear-medium effects in  $A+A(B)$  and  $p+A$  collisions, as well as improved constraints to differentiate between particle production models and to fine-tune event generators.

Particle production in  $A+A(B)$  collisions, is frequently described with thermodynamic and hydrodynamical models which utilize macroscopic variables such as temperature and entropy as model ingredients. This contrasts with the microscopic phenomenology (involving ladders of perturbative gluons, classical random gauge fields or strings, and parton hadronization) often used to characterize the soft collisions which account for the bulk of the particles produced in  $e^- + e^+$ ,  $e^\pm + p$ ,  $p(\bar{p})+p$  and  $p+A$  collisions [10–14]. The associated mechanisms, commonly classified as single-diffractive (SD) dissociation, double-diffractive (DD) dissociation and inelastic non-diffractive (ND) scattering in  $p(\bar{p})+p$  collisions [1], typically do not emphasize temperature and entropy as model elements.

Despite this predilection to use different theoretical model frameworks for  $p(\bar{p})+p$ ,  $p+A$  and  $A+A(B)$  collisions, it is well known that similar charged particle multiplicity ( $N_{\text{ch}}$ ) and pseudorapidity density ( $dN_{\text{ch}}/d\eta$ ) are obtained in  $p(\bar{p})+p$ , and peripheral  $A+A(B)$  and  $p+A$  collisions. Moreover, an azimuthal long-range (pseudorapidity difference  $|\Delta\eta| \geq 4$ ) two-particle angular correlation, akin to the “ridge” which results from collective

anisotropic flow in  $A+A$  collisions, has been observed in  $p+p$  and  $p+Pb$  collisions at the LHC [15–18], and in  $d+Au$  and  $He+Au$  collisions at RHIC [19, 20]. Qualitative consistency with these data has also been achieved in initial attempts to describe the amplitudes of these correlations hydrodynamically [19–21]. Thus, an important open question is whether equilibrium dynamics, linked to a common underlying particle production mechanism, dominates for these systems?

In this work, we use the available  $dN_{\text{ch}}/d\eta$  measurements for  $p+p$ ,  $p+A$  and  $A+A(B)$  collisions, as well as the  $\langle N_{\text{ch}} \rangle$  measurements for  $e^- + e^+$ ,  $e^\pm + p$ , and  $p(\bar{p})+p$  collisions to search for scaling patterns which could signal such an underlying particle production mechanism.

Our scaling analysis employs the macroscopic entropy ( $S$ ) ansatz

$$S \sim (TR)^3 \sim \text{const.}, \quad (1)$$

to capture the underlying physics of particle production, where  $T$  is the temperature,  $R$  is a characteristic size related to the volume, and  $dN_{\text{ch}}/d\eta$  and  $\langle N_{\text{ch}} \rangle$  are both proportional to  $S$ . A further simplification,  $N_{\text{pp}}^{1/3} \propto R$ , can be used to relate the number of participant pairs  $N_{\text{pp}}$ , to the initial volume. These pairs can be specified as colliding participant pairs (*e.g.*  $N_{\text{pp}} = 1$  for  $e^- + e^+$ ,  $e^\pm + p$  and  $p(\bar{p})+p$  collisions), nucleon participant pairs ( $N_{\text{npp}}$ ) or quark participant pairs ( $N_{\text{qpp}}$ ). For  $p+p$ ,  $p+A$  and  $A+A(B)$  collisions, Monte Carlo Glauber (MC-Glauber) calculations [31–36], were performed for several collision centralities at each beam energy to obtain  $N_{\text{npp}}$  and  $N_{\text{qpp}}$ . In each of these calculations, a subset  $N_{\text{np}} = 2N_{\text{npp}}$  ( $N_{\text{qp}} = 2N_{\text{qpp}}$ ) of the nucleons (quarks) become participants in each collision by undergoing an

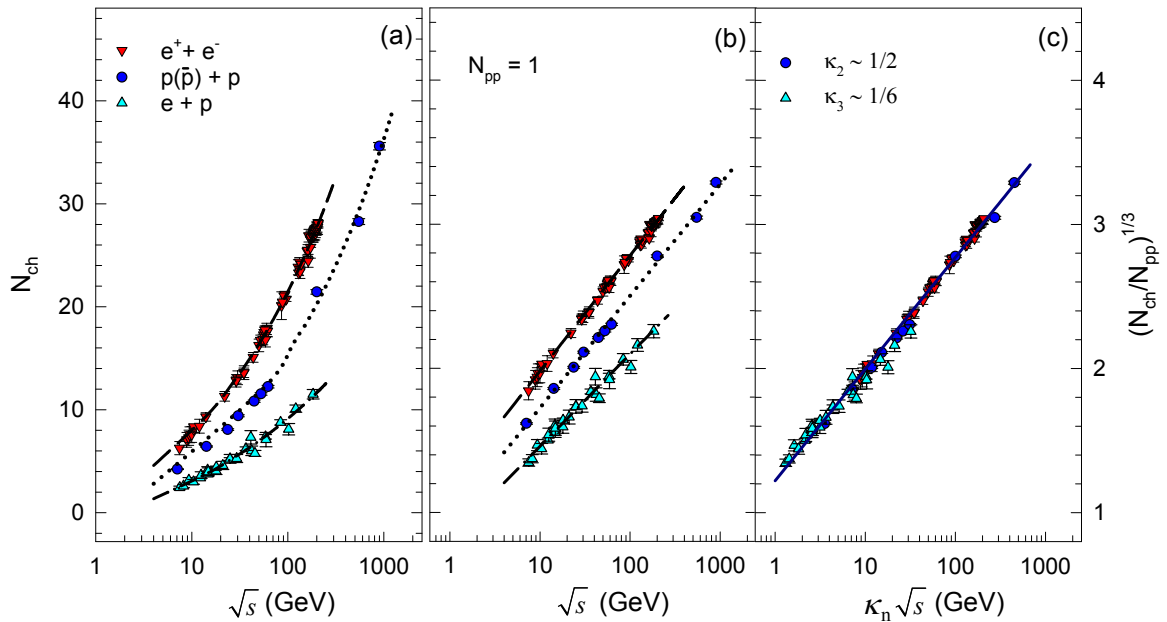


FIG. 1. (a)  $\langle N_{\text{ch}} \rangle$  vs.  $\sqrt{s}$  for  $e^- + e^+$  [22],  $p(\bar{p})+p$  [23–27] and  $e^\pm + p$  [28–30] collisions; (b)  $[(N_{\text{ch}})/N_{\text{pp}}]^{1/3}$  vs.  $\sqrt{s}$ ; (c)  $[(N_{\text{ch}})/N_{\text{pp}}]^{1/3}$  vs.  $\kappa_n \sqrt{s}$  for the  $\kappa_n$  values indicated. The curves are drawn to guide the eye.

initial inelastic N+N (q+q) interaction. The N+N (q+q) cross sections used in these calculations were obtained from the data systematics reported in Ref. [37].

Equation 1 suggests similar characteristic patterns for  $[(dN_{\text{ch}}/d\eta)/N_{\text{pp}}]^{1/3}$  and  $[(N_{\text{ch}})/N_{\text{pp}}]^{1/3}$  as a function of centrality and  $\sqrt{s}$  for all collision systems. We use this scaling ansatz in conjunction with the wealth of measurements spanning several orders of magnitude in  $\sqrt{s}$ , to search for, and study these predicted patterns.

The  $\langle N_{\text{ch}} \rangle$  measurements for  $e^- + e^+$ ,  $e^\pm + p$ , and  $p(\bar{p})+p$  collisions are shown in Fig. 1(a). They indicate a nonlinear increase with  $\log(\sqrt{s})$ , with  $\langle N_{\text{ch}} \rangle_{ee} > \langle N_{\text{ch}} \rangle_{pp} > \langle N_{\text{ch}} \rangle_{ep}$  at each value of  $\sqrt{s}$ . In contrast, Fig. 1(b) shows a linear increase of  $[(N_{\text{ch}})/N_{\text{pp}}]^{1/3}$  ( $N_{\text{pp}} = 1$ ) with  $\log(\sqrt{s})$ , suggesting a linear increase of  $T$  with  $\log(\sqrt{s})$ . Fig. 1(b) also indicates comparable slopes for  $[(N_{\text{ch}})/N_{\text{pp}}]^{1/3}$  vs.  $\log(\sqrt{s})$  for  $e^- + e^+$ ,  $e^\pm + p$ , and  $p(\bar{p})+p$  collisions, albeit with different magnitudes for  $[(N_{\text{ch}})/N_{\text{pp}}]^{1/3}$ . This similarity is compatible with the notion of an effective energy  $E_{\text{eff}}$  in  $p(\bar{p})+p$  and  $e^\pm + p$  collisions, available for particle production [49–52]. The remaining energy is associated with the leading particle/s which emerge at small angles with respect to the beam direction - the so-called leading particle effect [53]. In a constituent quark picture [54], only a fraction of the available quarks in  $p(\bar{p})+p$  and  $e^\pm + p$  collisions, contribute to  $E_{\text{eff}}$ . Thus,  $\sqrt{s_{ee}} \approx \kappa_2 \sqrt{s_{pp}} \approx \kappa_3 \sqrt{s_{ep}}$  ( $\kappa_1 = 1$ ) would be expected to give similar values for  $E_{\text{eff}}$  [55] and hence, comparable  $\langle N_{\text{ch}} \rangle$  values in  $e^- + e^+$ ,  $p(\bar{p})+p$  and  $e^\pm + p$  collisions. Here,  $\kappa_{2,3}$  are scale factors that are related to the number of quark participants and hence, the fraction of the available c.m energy which contribute to particle

production.

Figure 1(c) validates this leading particle effect. It shows that the disparate magnitudes of  $[(N_{\text{ch}})/N_{\text{pp}}]^{1/3}$  vs.  $\sqrt{s}$  for  $e^- + e^+$ ,  $p(\bar{p})+p$  and  $e^\pm + p$  collisions (cf. Fig. 1(b)) scale to a single curve for  $[(N_{\text{ch}})/N_{\text{pp}}]^{1/3}$  vs.  $\kappa_n \sqrt{s}$  where  $\kappa_1 = 1$ ,  $\kappa_2 \sim 1/2$  and  $\kappa_3 \sim 1/6$ . The values for  $\kappa_{2,3}$  validate the important role of quark participants in  $p(\bar{p})+p$  and  $e^\pm + p$  collisions. A fit to the data in Fig. 1(c) gives the expression

$$\langle N_{\text{ch}} \rangle = [b_{\langle N_{\text{ch}} \rangle} + m_{\langle N_{\text{ch}} \rangle} \log(\kappa_n \sqrt{s})]^3, \quad (2)$$

$$b_{\langle N_{\text{ch}} \rangle} = 1.22 \pm 0.01, \quad m_{\langle N_{\text{ch}} \rangle} = 0.775 \pm 0.006,$$

which can be used to predict  $\langle N_{\text{ch}} \rangle$  as a function of  $\sqrt{s}$ , for  $e^- + e^+$ ,  $e^\pm + p$ , and  $p(\bar{p})+p$  collisions.

Figures 2(a) and 3(a) show  $dN_{\text{ch}}/d\eta|_{\eta \approx 0}$  measurements for inelastic (INE) and non-single-diffractive (NSD) p+p collisions (respectively) for beam energies spanning the range  $\sqrt{s_{\text{NN}}} \sim 15 \text{ GeV} - 13 \text{ TeV}$ ; they indicate a monotonic increase of  $dN_{\text{ch}}/d\eta|_{\eta \approx 0}$  with  $\sqrt{s_{\text{NN}}}$  similar to that observed for  $\langle N_{\text{ch}} \rangle$  in Fig. 1(a). Figs. 2(b) and 3(b), by contrast, confirms the expected linear growth of  $[(dN_{\text{ch}}/d\eta|_{\eta \approx 0})/N_{\text{pp}}]^{1/3}$  with  $\log(\sqrt{s_{\text{NN}}})$ . The open points and dotted curves in these figures, affirm the expected trend for the  $\sqrt{s}$  dependence of  $[(dN_{\text{ch}}/d\eta|_{\eta \approx 0})/N_{\text{pp}}]^{1/3}$ . Here, the change in magnitude largely reflects the difference in the proportionality constants for  $N_{\text{pp}}$  and  $N_{\text{qpp}}$  (i.e.,  $N_{\text{pp}}^{1/3} \propto R$ ). The fits, indicated by the dashed curves in Figs. 2(b) and 3(b),

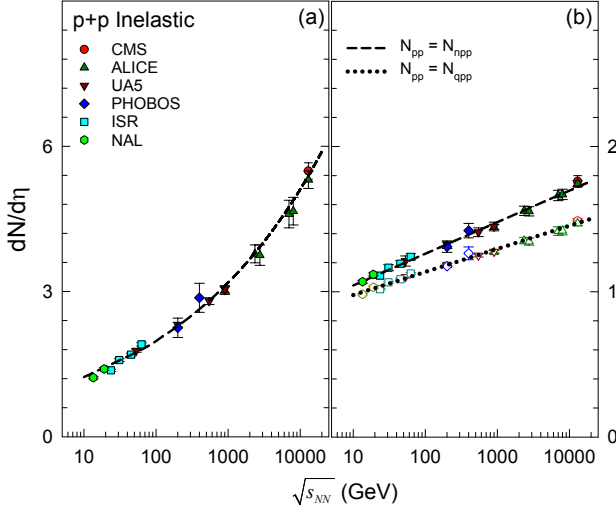


FIG. 2. (a)  $dN_{\text{ch}}/d\eta|_{\eta \approx 0}$  vs.  $\sqrt{s_{\text{NN}}}$  and (b)  $[(dN_{\text{ch}}/d\eta)/N_{\text{pp}}]^{1/3}$  vs.  $\sqrt{s_{\text{NN}}}$ , for p+p inelastic measurements from CMS [38], ALICE [39–41], UA5 [42], PHOBOS [43], ISR [25] and NAL Bubble Chamber [44]. The error bars include systematic uncertainties, when available. The curves in panel (b) represent fits to the data (see text).

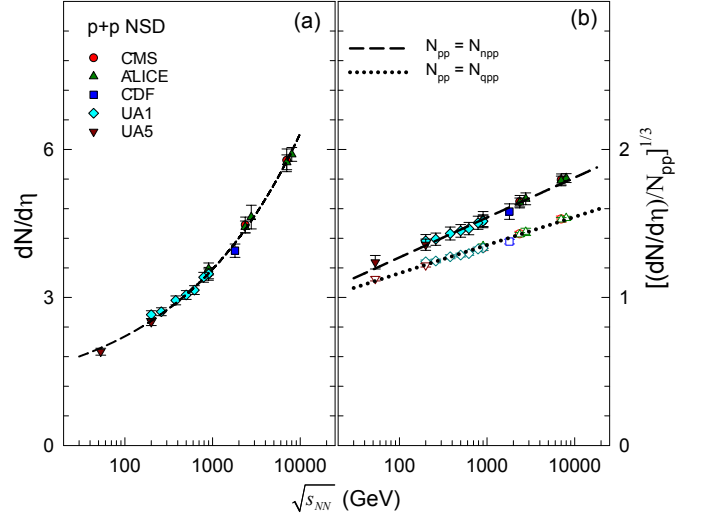


FIG. 3. (a)  $dN_{\text{ch}}/d\eta|_{\eta \approx 0}$  vs.  $\sqrt{s_{\text{NN}}}$  and (b)  $[(dN_{\text{ch}}/d\eta)/N_{\text{pp}}]^{1/3}$  vs.  $\sqrt{s_{\text{NN}}}$ , for p+p NSD measurements from CMS [45], ALICE [40], CDF [46], UA1 [47] and UA5 [42]. The error bars include the available systematic uncertainties. The curves in panel (b) represent fits to the data (see text).

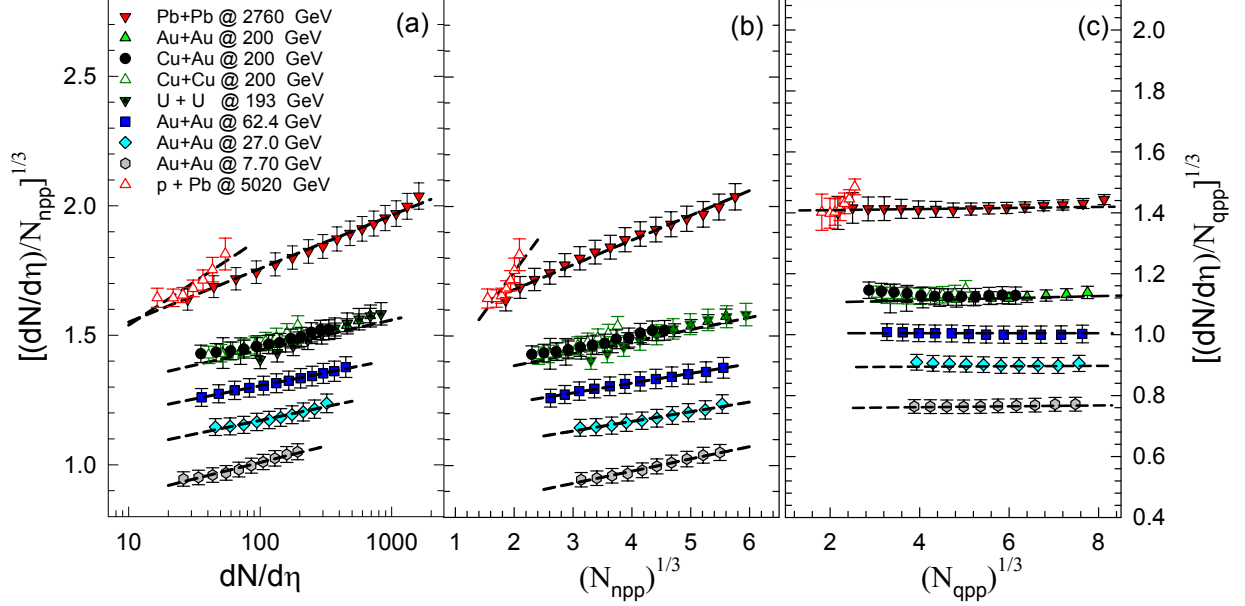


FIG. 4. (a)  $[(dN_{\text{ch}}/d\eta)|_{|\eta|=0.5}/N_{\text{npp}}]^{1/3}$  vs.  $dN_{\text{ch}}/d\eta$ ; (b)  $[(dN_{\text{ch}}/d\eta)|_{|\eta|=0.5}/N_{\text{npp}}]^{1/3}$  vs.  $N_{\text{npp}}^{1/3}$ ; (c)  $[(dN_{\text{ch}}/d\eta)|_{|\eta|=0.5}/N_{\text{qpp}}]^{1/3}$  vs.  $N_{\text{qpp}}^{1/3}$ . Results are shown for several systems and  $\sqrt{s_{\text{NN}}}$  values as indicated. The data are obtained from Refs. [4–9, 48]. The curves are drawn to guide the eye.

give the expressions

$$dN_{\text{ch}}/d\eta|_{\text{INE}} = [b_{\text{INE}} + m_{\text{INE}} \log(\sqrt{s_{\text{NN}}})]^3, \quad (3)$$

$$b_{\text{INE}} = 0.826 \pm 0.008, \quad m_{\text{INE}} = 0.220 \pm 0.004,$$

$$dN_{\text{ch}}/d\eta|_{\text{NSD}} = [b_{\text{NSD}} + m_{\text{NSD}} \log(\sqrt{s_{\text{NN}}})]^3, \quad (4)$$

$$b_{\text{NSD}} = 0.747 \pm 0.022, \quad m_{\text{NSD}} = 0.267 \pm 0.007,$$

for the mid-pseudorapidity density for INE and NSD p+p collisions. Here, it is noteworthy that the recent inelastic p+p measurements at  $\sqrt{s_{\text{NN}}} = 13$  TeV by the CMS [38] and ALICE [41] collaborations are in very good agree-

ment with the scaling prediction shown in Fig. 2(b). The data trends in Figs. 1(c), 2(b) and 3(b) also suggest that the mean transverse momentum ( $\langle p_T \rangle \propto T$ ) for the particles emitted in these collisions, increase as  $\log(\sqrt{s})$ .

The scaling properties for p+A and A+A(B) collisions are summarized in Fig. 4 where illustrative plots of  $[(dN_{\text{ch}}/d\eta|_{|\eta|=0.5})/N_{\text{npp}}]^{1/3}$  vs.  $dN_{\text{ch}}/d\eta$  and  $N_{\text{npp}}^{1/3}$ , and  $[(dN_{\text{ch}}/d\eta|_{|\eta|=0.5})/N_{\text{qpp}}]^{1/3}$  vs.  $N_{\text{qpp}}^{1/3}$  are shown. Analogous plots were obtained for other collision systems and beam energies. Figs. 4(a) and 4(b) show that, irrespective of the collision system,  $[(dN_{\text{ch}}/d\eta|_{|\eta|=0.5})/N_{\text{npp}}]^{1/3}$  increases as  $\log(dN_{\text{ch}}/d\eta)$  ( $N_{\text{npp}}^{1/3}$ ), suggesting that  $T$  has a logarithmic (linear) dependence on the pseudorapidity density (size) at a given value of  $\sqrt{s_{\text{NN}}}$ ; note the slope increase with beam energy, as well as the lack of sensitivity to system type (Cu+Cu, Cu+Au, Au+Au, U+U), for a fixed value of  $\sqrt{s_{\text{NN}}}$ . These results suggest that, in addition to the expected increase with  $\sqrt{s_{\text{NN}}}$ , the mean transverse momentum  $\langle p_T \rangle$  or transverse mass  $\langle m_T \rangle$  of the emitted particles, should increase as  $\log(dN_{\text{ch}}/d\eta)$  at a given value of  $\sqrt{s_{\text{NN}}}$ . They also suggest that the pseudorapidity density factorizes into contributions which depend on  $\sqrt{s_{\text{NN}}}$  and  $N_{\text{npp}}^{1/3}$  respectively. Indeed, the data sets shown for each  $\sqrt{s_{\text{NN}}}$  in Fig. 4(b), can be scaled to a single curve with scaling factors that are proportional to  $\log(\sqrt{s_{\text{NN}}})$ .

Figure 4(c) contrasts with Figs. 4(a) and 4(b). It shows that, when  $N_{\text{qpp}}$  is used instead of  $N_{\text{npp}}$ , the size dependence of  $[(dN_{\text{ch}}/d\eta|_{|\eta|=0.5})/N_{\text{npp}}]^{1/3}$ , apparent in Fig. 4(b), is suppressed (but not its  $\sqrt{s_{\text{NN}}}$  dependence). We attribute the flat dependence of  $[(dN_{\text{ch}}/d\eta|_{|\eta|=0.5})/N_{\text{qpp}}]^{1/3}$  on size ( $N_{\text{npp}}^{1/3}$  or  $N_{\text{qpp}}^{1/3}$ ), to the linear dependence of  $N_{\text{qp}}/N_{\text{npp}}$  on initial size as illustrated in Fig. 5(a) for Pb+Pb and Au+Au collisions. Note that for central and mid-central p+Pb collisions,  $N_{\text{qp}}/N_{\text{npp}}$  decreases with  $N_{\text{npp}}^{1/3}$ ; this results in a reduction of the energy deposited in these collisions, as well as large multiplicity fluctuations.

The  $\sqrt{s_{\text{NN}}}$  dependence of  $[(dN_{\text{ch}}/d\eta|_{|\eta|=0.5})/N_{\text{qpp}}]^{1/3}$  for A+A(B) and NSD p+p collisions are compared in Fig. 5(b). The comparison indicates strikingly similar trends for NSD p+p, and A+A(B) collisions, as would be expected for a common underlying particle production mechanism in these collisions. Note that for  $\sqrt{s_{\text{NN}}} \lesssim 2$  TeV, higher temperatures [and larger  $\langle p_T \rangle$ ] are implied for the smaller p+p collision systems. Figs. 4(c) and 5(b) also indicate that the centrality and  $\sqrt{s}$  dependent values of  $dN_{\text{ch}}/d\eta|_{|\eta|=0.5}$ , obtained for different collision systems, scale as  $N_{\text{qpp}}$  and  $\log(\sqrt{s_{\text{NN}}})$ . A fit to the A+A(B) data in Fig. 5(b), gives the expression

$$dN_{\text{ch}}/d\eta|_{|\eta|=0.5} = N_{\text{qpp}} [b_{\text{AA}} + m_{\text{AA}} \log(\sqrt{s})]^3, \quad (5)$$

$$b_{\text{AA}} = 0.530 \pm 0.008, \quad m_{\text{AA}} = 0.258 \pm 0.004,$$

which systematizes the collision energy and centrality dependencies of the pseudorapidity density in A+A(B)

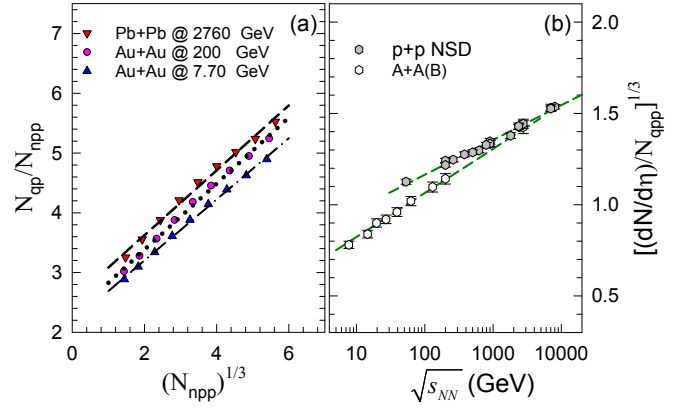


FIG. 5. (a)  $N_{\text{qp}}/N_{\text{npp}}$  vs.  $N_{\text{npp}}^{1/3}$  for Au+Au and Pb+Pb collisions; (b)  $[(dN_{\text{ch}}/d\eta|_{|\eta|=0.5})/N_{\text{qpp}}]^{1/3}$  vs.  $\sqrt{s_{\text{NN}}}$  for NSD p+p and A+A(B) collisions as indicated.

collisions across the full range of beam energies. Eq. 5 provides a basis for robust predictions of the value of  $dN_{\text{ch}}/d\eta|_{|\eta|=0.5}$  as a function of  $N_{\text{qpp}}$  and  $\sqrt{s}$  across systems and collision energies. For example, it predicts an  $\sim 20\%$  increase in the  $dN_{\text{ch}}/d\eta|_{|\eta|=0.5}$  values for Pb+Pb collisions (across centralities) at 5.02 TeV, compared to the same measurement at 2.76 TeV. This increase reflects the respective contributions linked to the increase in the value of  $\sqrt{s}$  and the small growth in the magnitudes of  $N_{\text{qpp}}$ .

In summary, we have performed a systematic study of the scaling properties of  $dN_{\text{ch}}/d\eta$  measurements for p+p, p+A and A+A(B) collisions, and  $\langle N_{\text{ch}} \rangle$  measurements for  $e^- + e^+$ ,  $e^\pm + p$ , and  $p(\bar{p})+p$  collisions, to investigate the mechanism for particle production in these collisions. The wealth of the measurements, spanning several orders of magnitude in  $\sqrt{s}$ , indicate characteristic scaling patterns for both  $dN_{\text{ch}}/d\eta$  and  $\langle N_{\text{ch}} \rangle$ , suggestive of a common underlying entropy production mechanism for these systems. The scaling patterns for  $\langle N_{\text{ch}} \rangle$  validate the essential role of the leading particle effect in  $p(\bar{p})+p$  and  $e^\pm + p$  collisions and the importance of quark participants in A+A(B) collisions. The patterns for the scaled values of  $dN_{\text{ch}}/d\eta$  and  $\langle N_{\text{ch}} \rangle$  indicate strikingly similar trends for NSD p+p and A+A(B) collisions, and show that the pseudorapidity density and the  $\langle N_{\text{ch}} \rangle$  for  $e^- + e^+$ ,  $e^\pm + p$ , p+p, and A+A(B) collisions, factorize into contributions which depend on  $\log(\sqrt{s})$  and  $N_{\text{pp}}$  respectively. The quantification of these scaling patterns, give expressions which serve to systematize the  $dN_{\text{ch}}/d\eta$  and  $\langle N_{\text{ch}} \rangle$  measurements for  $e^- + e^+$ ,  $e^\pm + p$ ,  $p(\bar{p})+p$ , p+A and A+A(B) collisions, and to predict their magnitudes as a function of  $N_{\text{pp}}$  and  $\sqrt{s}$ . These scaling results have important utility in the study of a broad array of observables which are currently being pursued at both RHIC and the LHC.

## ACKNOWLEDGMENTS

This research is supported by the US DOE under contract DE-FG02-87ER40331.A008.

\* E-mail: Roy.Lacey@Stonybrook.edu

- [1] W. Kittel and E. A. DeWolf, *Soft Multihadron Dynamics* (World Scientific, Singapore, 2005), ISBN 981-256-295-8.
- [2] N. Armesto, N. Borghini, S. Jeon, U. A. Wiedemann, S. Abreu, V. Akkelin, J. Alam, J. L. Albacete, A. Andronic, D. Antonov, et al., *J. Phys.* **G35**, 054001 (2008), 0711.0974.
- [3] J. F. Grosse-Oetringhaus and K. Reygers, *J. Phys.* **G37**, 083001 (2010), 0912.0023.
- [4] B. Alver et al. (PHOBOS), *Phys. Rev.* **C83**, 024913 (2011), 1011.1940.
- [5] K. Aamodt et al. (ALICE), *Phys. Rev. Lett.* **106**, 032301 (2011), 1012.1657.
- [6] S. Chatrchyan et al. (CMS), *JHEP* **08**, 141 (2011), 1107.4800.
- [7] G. Aad et al. (ATLAS), *Phys. Lett.* **B710**, 363 (2012), 1108.6027.
- [8] L. Adamczyk et al. (STAR), *Phys. Rev.* **C86**, 054908 (2012), 1206.5528.
- [9] A. Adare et al. (2015), 1509.06727.
- [10] D. Kharzeev, E. Levin, and M. Nardi, *Nucl. Phys.* **A747**, 609 (2005), hep-ph/0408050.
- [11] N. Armesto, C. A. Salgado, and U. A. Wiedemann, *Phys. Rev. Lett.* **94**, 022002 (2005), hep-ph/0407018.
- [12] M. G. Albrow et al. (TeV4LHC QCD Working Group) (2006), hep-ph/0610012, URL [http://lss.fnal.gov/cgi-bin/find\\_paper.pl?conf-06-359](http://lss.fnal.gov/cgi-bin/find_paper.pl?conf-06-359)
- [13] K. Werner, *Nucl. Phys. Proc. Suppl.* **175-176**, 81 (2008).
- [14] K. Dusling and R. Venugopalan, *Phys. Rev.* **D87**, 054014 (2013), 1211.3701.
- [15] V. Khachatryan et al. (CMS), *JHEP* **09**, 091 (2010), 1009.4122.
- [16] B. Abelev et al. (ALICE), *Phys. Lett.* **B719**, 29 (2013), 1212.2001.
- [17] G. Aad et al. (ATLAS), *Phys. Rev. Lett.* **110**, 182302 (2013), 1212.5198.
- [18] S. Chatrchyan et al. (CMS), *Phys. Lett.* **B718**, 795 (2013), 1210.5482.
- [19] A. Adare et al. (PHENIX), *Phys. Rev. Lett.* **114**, 192301 (2015), 1404.7461.
- [20] A. Adare et al. (PHENIX), *Phys. Rev. Lett.* **115**, 142301 (2015), 1507.06273.
- [21] P. Bozek, *Phys. Rev.* **C85**, 014911 (2012), 1112.0915.
- [22] K. Nakamura et al. (Particle Data Group), *J. Phys.* **G37**, 075021 (2010).
- [23] J. Benecke and et al. (Bonn-Hamburg-Munich), *Nucl. Phys.* **B76**, 29 (1974).
- [24] W. M. Morse, V. E. Barnes, D. D. Carmony, R. S. Christian, A. F. Garfinkel, L. K. Rangan, A. R. Erwin, E. H. Harvey, R. J. Loveless, and M. A. Thompson, *Phys. Rev.* **D15**, 66 (1977).
- [25] A. Breakstone et al. (Ames-Bologna-CERN-Dortmund-Heidelberg-Warsaw), *Phys. Rev.* **D30**, 528 (1984).
- [26] G. J. Alner et al. (UA5), *Phys. Lett.* **B167**, 476 (1986).
- [27] R. E. Ansorge et al. (UA5), *Z. Phys.* **C43**, 357 (1989).
- [28] C. Adloff et al. (H1), *Nucl. Phys.* **B504**, 3 (1997), hep-ex/9707005.
- [29] J. Breitweg et al. (ZEUS), *Eur. Phys. J.* **C11**, 251 (1999), hep-ex/9903056.
- [30] S. Chekanov et al. (ZEUS), *Phys. Lett.* **B510**, 36 (2001), hep-ex/0104036.
- [31] M. L. Miller, K. Reygers, S. J. Sanders, and P. Steinberg, *Ann. Rev. Nucl. Part. Sci.* **57**, 205 (2007).
- [32] R. A. Lacey, R. Wei, N. Ajitanand, and A. Taranenko, *Phys. Rev.* **C83**, 044902 (2011), 1009.5230.
- [33] S. Eremin and S. Voloshin, *Phys. Rev.* **C67**, 064905 (2003), nucl-th/0302071.
- [34] A. Bialas and A. Bzdak, *Phys. Lett.* **B649**, 263 (2007), nucl-th/0611021.
- [35] R. Nouicer, *Eur. Phys. J.* **C49**, 281 (2007), nucl-th/0608038.
- [36] S. S. Adler et al. (PHENIX), *Phys. Rev.* **C89**, 044905 (2014), 1312.6676.
- [37] D. A. Fagundes, M. J. Menon, and P. V. R. G. Silva, *J. Phys.* **G40**, 065005 (2013), 1208.3456.
- [38] V. Khachatryan et al. (CMS), *Phys. Lett.* **B751**, 143 (2015), 1507.05915.
- [39] K. Aamodt et al. (ALICE), *Eur. Phys. J.* **C68**, 89 (2010), 1004.3034.
- [40] J. Adam et al. (ALICE) (2015), 1509.07541.
- [41] J. Adam et al. (ALICE) (2015), 1509.08734.
- [42] G. J. Alner et al. (UA5), *Z. Phys.* **C33**, 1 (1986).
- [43] R. Nouicer et al. (PHOBOS), *J. Phys.* **G30**, S1133 (2004), nucl-ex/0403033.
- [44] J. Whitmore, *Phys. Rept.* **10**, 273 (1974).
- [45] V. Khachatryan et al. (CMS), *Phys. Rev. Lett.* **105**, 022002 (2010), 1005.3299.
- [46] F. Abe et al. (CDF), *Phys. Rev.* **D41**, 2330 (1990), [,119(1989)].
- [47] C. Albajar et al. (UA1), *Nucl. Phys.* **B335**, 261 (1990).
- [48] G. Aad et al. (ATLAS) (2015), 1508.00848.
- [49] E. L. Feinberg, *Phys. Rept.* **5**, 237 (1972).
- [50] E. Albini, P. Capiluppi, G. Giacomelli, and A. M. Rossi, *Nuovo Cim.* **A32**, 101 (1976).
- [51] M. Basile et al., *Phys. Lett.* **B92**, 367 (1980).
- [52] M. Basile et al., *Nuovo Cim.* **A67**, 244 (1982).
- [53] B. B. Back et al. (PHOBOS) (2003), nucl-ex/0301017.
- [54] J. Nyiri, *Int. J. Mod. Phys.* **A18**, 2403 (2003), hep-ph/0207155.
- [55] E. K. G. Sarkisyan and A. S. Sakharov (2004), hep-ph/0410324.